Turn Around Point Long Period Fiber Gratings With Coupling to Asymmetric Cladding Modes Fabricated by a Femtosecond Laser and Coated With Titanium Dioxide

Duarte Viveiros, José Manuel Marques Martins de Almeida, Luís Coelho, Helena Vasconcelos, João M. Maia, Vítor A. Amorim, Pedro A. S. Jorge, and Paulo V. S. Marques

***Abstract*—A detailed study of turn around point (TAP) long period fiber gratings (LPFGs) with coupling to the asymmetric cladding modes of a standard single-mode fiber (SMF-28e), fabricated by femtosecond (fs) laser direct writing was realized. The entire fabrication process, including the coating with different titanium dioxide (TiO_2) film thicknesses of LPFGs and the corrections needed to achieve coated devices operating precisely in the TAP condition with coupling to the asymmetric cladding modes, was addressed. The significant fabrication details are also given, such as inscription periods, shape and localization of the refractive index modifications across the core. The fabrication process described allows the optimization of the LPFGs sensitivity in regards to the surrounding refractive index (SRI). Optimization of the writing parameters to obtain gratings working at the TAP for two different media surrounding the fiber (water and air) was achieved. It was demonstrated that for a grating period of 191.8 μm, the $LP_{1,12}$ mode exhibits a TAP at 1442.7 nm in air, and for a period of 192.5 μm, the same mode exhibits a TAP at 1448.6 nm in water. The LPFGs operating at the TAP in air and water were coated with 10, 20, and 30 nm thin TiO_2 film thicknesses and the spectral behavior characterized. The wavelength sensitivity to the surrounding refractive index (SRI) was assessed in the range between 1.3700 to 1.4120, and a maximum sensitivity of ~8051.4 nm/RIU was measured for the 192.5 μm LPFG coated with a 30 nm thick TiO_2 film.**

***Index Terms*—Femtosecond laser direct writing, optical fiber sensors, refractive index sensing, titanium dioxide thin films, turn around point long period fiber gratings.**

Manuscript received October 20, 2020; revised February 28, 2021 and March 25, 2021; accepted May 2, 2021. Date of publication May 7, 2021; date of current version July 16, 2021. This work was supported in part by the Ministry of Education and Science of Portuguese Government under Grant SFRH/BD/110035/2015 and in part by Project "On Chip Whispering Gallery Mode Optical Microcavities For Emerging Microcontaminant Determination In Waters" - SAFE WATER, which is supported and co-funded by European Commission, Directorate-General Communications Networks, Content and Technology (DG CONNECT) under the ERA-NET Cofund scheme - Horizon 2020 "Horizon 2020 – the Framework Programme for Research and Innovation (2014-2020)", under Grant 7859/BI_B2-C/2019. *(Corresponding author: Duarte Viveiros.)*

Duarte Viveiros, João M. Maia, Vítor A. Amorim, Pedro A. S. Jorge, and Paulo V. S. Marques are with the Centre for Applied Photonics (CAP), INESC TEC, 4150-179 Porto, Portugal, and also with the Department of Physics and Astronomy, Faculty of Science, University of Porto, 4169-007 Porto, Portugal (e-mail: carlos.d.viveiros@inesctec.pt; joao.m.maia@inesctec.pt; vitor.a.amorim@inesctec.pt; pedro.jorge@fc.up.pt; psmarque@fc.up.pt).

José Manuel Marques Martins de Almeida is with the Centre for Applied Photonics (CAP), INESC TEC, 4150-179 Porto, Portugal, and also with the Department of Physics, University of Trás-os-Montes e Alto Douro, 5001-801 Vila Real, Portugal (e-mail: jmmma@utad.pt).

Luís Coelho is with the Centre for Applied Photonics (CAP), INESC TEC, 4150-179 Porto, Portugal (e-mail: lcoelho@inesctec.p).

Helena Vasconcelos is with the Centre for Applied Photonics (CAP), INESC TEC, 4150-179 Porto, Portugal, and also with the Department of Physics, University of Trás-os-Montes e Alto Douro, 5001-801 Vila Real, Portugal (e-mail: helena.s.vasconcelos@inesctec.pt).

Color versions of one or more figures in this article are available at https://doi.org/10.1109/JLT.2021.3078257.

Digital Object Identifier 10.1109/JLT.2021.3078257

I. Introduction

LONG period fiber gratings (LPFGs) have been under continual investigation for at least forty years [1]. The fabrication of the LPFGs using several methods has been demonstrated, including exposure to UV and CO_2 laser radiation [2]–[5], electric arc discharge [6], laser ablation [7], mechanical pressure [8], and also femtosecond (fs) laser writing [9]–[11]. The LPFGs inscription in different optical fibers, such as photonic crystal fibers [12], standard single-mode optical fibers [11], polarization-maintaining fibers [13], and photosensitive fibers were also extensively explored [7], [13]. The LPFGs are induced by a periodic modulation of the refractive index (RI) along the longitudinal axis of an optical fiber with periods greater than 100 μm [1], [7], [14]. This modulation allows the coupling of light from the LP_{01} core-guided mode into forward-propagating cladding-guided modes ($LP_{l,m}$, linearly polarized modes with azimuthal and radial integer indices l and m, respectively) at or near-resonant wavelengths. The efficient coupling between the core mode and the co-propagating cladding modes occurs under the phase-matching condition, where the resonant wavelength of the LPFG, λ_{res}, is determined by [1], [8]:

$$\lambda_{res} = \left(n_{core}^{eff}(\lambda) - n_{cl\ l,m}^{eff}(\lambda)\right)\Lambda \tag{1}$$

where n_{core}^{eff} and $n_{cl\ l,m}^{eff}$ are the effective RI of the propagating core mode and m^{th} cladding modes, respectively, at wavelength λ, and $\wedge$ is the grating period. The resonance wavelength sensitivity of the LPFGs to external perturbations relies on the effective RIs and the grating period, underlying

to the propagation conditions in the core and cladding modes. The resonance wavelength shift caused by the changes in the effective RIs and the grating period allows the measurement of several parameters such as temperature, strain, and refractive index [1], [3], [8]. Regarding the LPFGs based RI sensors, they can be used efficiently in biological, chemical, and biochemical sensing applications [15], [16], [17]. The RI measure is defined as a shift of the resonance wavelength per RI Unit (RIU) [15]. The fabrication of LPFGs with high sensitivity to the surrounding refractive index (SRI) has been explored [16], [18], [19]. The methodologies reported include LPFGs operating in the turning around point (TAP) region, evanescent field enhancement by reducing cladding diameter, and mode transition (MT) [20] achieved by coating the LPFGs with a thin layer of material whose RI is higher than that of the cladding [16], [18], [19]. The high RI thin film coatings promote the transition between cladding guided modes in overlay guided modes inducing a re-distribution of the cladding modes, enhancing the evanescent wave interaction with the surrounding medium [16], [18], [19]. In addition, a combination of these methods by selecting a period very close to the TAP and making the fine tunning to operate precisely in the TAP by reducing the cladding diameter or by coating with a thin layer of material could further improve the SRI sensitivity of the LPFGs sensors [16], [18], [19].

The fabrication of LPFGs operating at the TAP without the use of post-fabrication technics (i.e., chemical etching to fine-tune the LPFGs operation around TAP) has proven to be a challenge, corroborated by the few manuscripts reported so far [2], [3], [11], [16], [21]. In addition, the fabrication of LPFGs operating at the TAP of asymmetric cladding modes for SRI sensing has not been discussed in detail; nevertheless, to our knowledge, fabrication of LPFGs allowing the coupling to asymmetric cladding mode was only demonstrated in [6], [22], [23].

The SRI sensitivity of the LPFGs sensors could be further improved, selecting a high RI thin film, such as titanium dioxide (TiO_2). TiO_2 is non-toxic and biocompatible, exhibits low optical absorption, is mechanically resistant, and supports high temperature and electrical fields [16], [24]. Several optical fiber sensors based on LPFGs [16], [24]–[29], Mach-Zehnder Interferometers [30], and fiber Bragg gratings [31], mainly fabricated by exposure to UV and CO_2 laser radiation, and electric arc discharge, were coated with TiO_2 thin films given the advantages shown. However, the fs-laser fabrication of LPFGs operating in the TAP with coupling to asymmetric cladding modes and coated with TiO_2 thin films has not been systematically studied.

In this work, the entire fabrication process, including the coating with different TiO_2 film thicknesses, and characterization of the TAP LPFGs in SMF-28e fibers inscribed by fs-laser direct writing, is described. The impact of the fabrication parameters in the coupling behavior was studied in order to improve the coupling efficiency and obtain an LPFG in the TAP condition surrounded by air or water. The change in the effective RI of the asymmetric $LP_{1,12}$ cladding mode as a function of the TiO_2 film thicknesses was evaluated through simulation and experimentally. The resonance wavelength sensitivity to the SRI of the uncoated and TiO_2 coated LPFGs operating at the TAP in air and water was evaluated and compared to the literature's reported works.

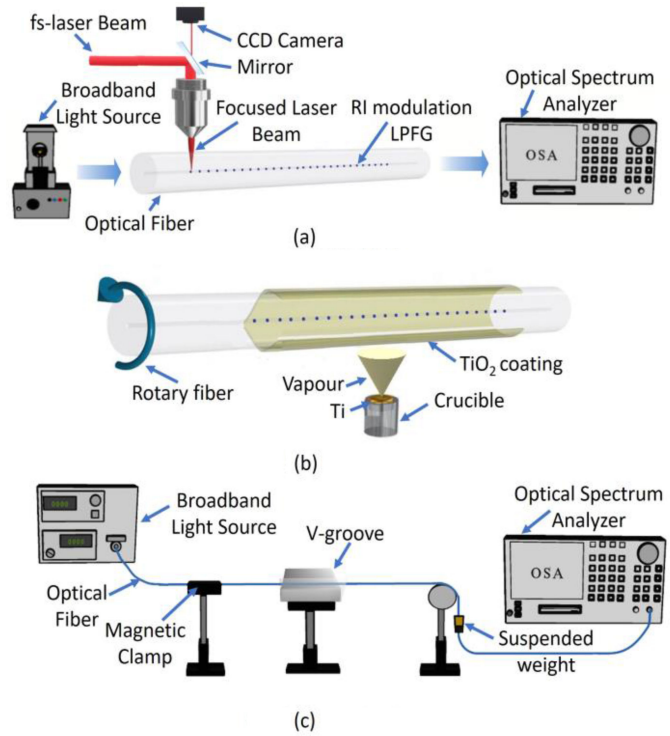

Fig. 1. Schematic illustration of the LPFGs: (a) Fabrication, (b) coating, and (c) characterization procedures.

II. Materials and Methods

The laser direct writing system assembled employs a fiber amplified fs-laser (Satsuma HP, from Amplitude Systèmes), operating at 515 nm with a pulse duration of $\approx$ 250 fs at a repetition rate of 500 kHz. A 40$\times$ aspherical lens (Newport 5722-A-H) with a numerical aperture of NA = 0.5 was used for focusing the laser beam inside the SMF-28e Corning fiber core. The lens was mounted in a Y (Newport M-ILS150CC) and Z (Newport VP-25XA) precision linear stages, which allow motion in the direction transversal to the fiber axis and the beam propagation direction, respectively. A high-quality X air-bearing linear stage (Aerotech ABL10100-LN) with a resolution of 0.5 nm was utilized to scan the optical fiber. The laser beam polarization was adjusted to be parallel to the scanning X direction, which is parallel to the fiber axis. The optical fiber without coating was held by two clamps, where each one is part of a 3-axis positioner, mounted in the X-stage. The optical fiber was stretched and kept under constant tension (1 N) during the fabrication. The real-time monitoring and the adjustment of the fabrication tension were realized through a calibrated load cell (Interface SML series). The precise positioning of the grating in the fiber core was realized using the image on the CCD camera acquired through the writing lens, as illustrated in Fig. 1(a). The focal positions within the fiber were adjusted through the back-reflected laser beam from the fiber surface, tracking a single bright spot when the laser focus is positioned at the top center position of the fiber cladding.

For writing TAP LPFGs, the laser gate was externally controlled by a periodic square time function with a duty cycle of

50% generated by the synthesized function generator (DS345, Stanford Research Systems). Writing of gratings was achieved by translating the optical fiber at constant velocity (v) along X-axis, with the signal modulation turned on [11].

The spectral characteristics of the LPFGs were monitored in real-time by using an unpolarized broadband light source (BBS) and an Optical Spectrum Analyzer (OSA) model ANDO AQ-6315B, following the procedure described in [11].

The LPFGs were fabricated with different modulation periods, a 50 μm/s scan velocity, a fiber tension of 1 N, 40 mm long and with pulse energies of 120 and 140 nJ at a depth of 60 and 57 μm from the top center position of the fiber cladding, respectively. The LPFGs were annealed, according to the procedure reported in [11] before the TiO_2 thin film coating to ensure that the wavelength and the intensity of the resonance band remain unchanged with the temperature used in the deposition procedure.

The TiO_2 thin-film deposition around the TAP LPFG was done by thermal evaporation of pure titanium in a controlled oxygen atmosphere using an electron beam evaporator (Auto 306, Edwards Ltd, U.K.), following the procedure described in [19], [20], producing homogeneous TiO_2 films with thicknesses of 10, 20, and 30 nm, as illustrated in Fig. 1(b).

A RI characterization setup was prepared to measure the LPFGs spectrum using different surrounding mediums. The LPFGs were characterized in the transmission mode, keeping the fiber stretched at a constant tension produced by a suspended weight of 5.8 g and measuring the BBS normalized signal with the OSA without polarization control from 1200 to 1700 nm with a 2 nm resolution.

The LPFGs were introduced in a glass V-groove, parallel aligned to the fiber axis, and characterized with RI calibrated oils (Cargille-Sacher Laboratories Inc., USA), as illustrated in Fig. 1(c). The RI oils used belongs to the series AAA $n_D^{25°C} = 1.3000 - 1.3950 \pm 0.0002$ and AA $n_D^{25°C} = 1.4000 - 1.4580 \pm 0.0002$. After each measurement, both LPFG and the V-groove were cleaned with acetone to avoid contamination of the next SRI oil. The measurements were performed in a temperature-controlled environment, monitoring the temperature during the characterization with a type K thermocouple thermometer (AMECaL ST-9612).

To assess the stability and repeatability of the sensing scheme, the spectral resolution was calculated based on the method reported in [32]. The RI spectral resolution, *RRI*, was estimated considering the following expression [32]:

$$R_{RI} = \frac{\rho\sigma}{S_{RI}} \tag{2}$$

where ρ represents the confidence interval (99.7%), σ is the standard deviation of a set of measurements performed in repeatable and reproducible conditions associated with a step variation of the external RI, and S_{RI} is the sensitivity linked with the SRI measurement range.

III. Experimental Results and Discussion

A. Characterization of the TAP LPFGs Writing

Two 40 mm long LPFGs with a period of 191.8 μm were fabricated at a depth of 60 and 57 μm from the top center position of the fiber cladding with pulse energies of 120 and 140 nJ, respectively.

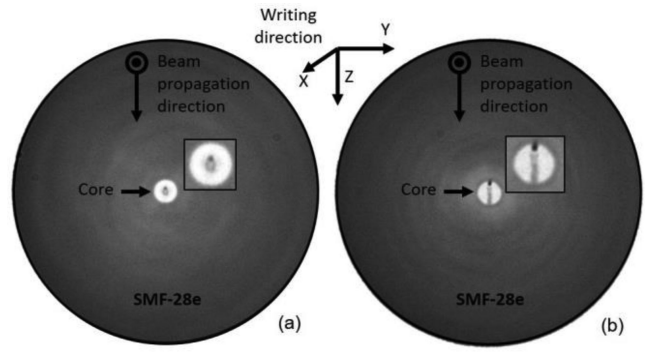

Fig. 2. Optical microscope views of the cross-sections of the fs-laser written LPFGs in the SMF-28e fiber (8.2 μm core diameter) at a depth from the fiber surface of (a) 60 μm with pulse energy of 120 nJ and (b) 57 μm with pulse energy of 140 nJ.

The shape of the fs-laser induced RI modification was assessed by cleaving the optical fibers and inspecting with an optical microscope (Leica DM6000 M) the cross-sections of the structures, as shown in Fig. 2.

Both types of fs-laser induced RI modifications are transversely inhomogeneous and asymmetric, resembling an elliptic and rectangular shape that extends across the core center, as shown in the insets of Fig. 2(a) and (b), respectively. The non-uniformity and localization of the RI modifications lead to coupling to the asymmetric $LP_{i,j}$ cladding modes of order *j*. For LPFGs written with periods between 175 and 200 μm coupling occurs to the asymmetric $LP_{1,12}$ cladding mode, accordingly with the simulated phase-matching curves reported in [6], and as addressed in a previous work [11].

LPFGs with periods between 190 and 193 μm were inscribed with the fabrication parameters aforementioned, to study the spectral behavior at, or very close to, the TAP of the asymmetric $LP_{1,12}$ cladding mode, considering the LPFGs surrounded by air and water. The LPFGs transmission spectra in air and water for the two fabrication conditions are shown in Fig. 3(a) and (b), respectively. For the grating period of 190 μm, the $LP_{1,12}$ mode exhibits two resonances at $\sim$1290.8 and $\sim$1600.2 nm ($\Delta\lambda = 309.4$ nm) in air, as shown in Fig. 3(a). When the grating inscription period increased from 190 to 191.7 μm, the two resonances approach, reaching a separation of 51.4 nm. As can be seen in Fig. 3(c), the 191.8 μm period matches the peak of the dispersion curve of the $LP_{1,12}$ cladding mode, where the two resonance bands in the transmission spectrum merge into one band at $\sim$1442.7 nm. Moreover, the increase of the inscription period to 192 μm results in a decrease of coupling efficiency, but not in wavelength, as shown in Fig. 3(c) and (d). For LPFGs fabricated with periods greater than 192 μm and surrounded by air, the resonance vanishes because the coupling occurs outside of the dispersion curve of the $LP_{1,12}$ cladding mode. However, if the SRI increase, i.e., when the LPFGs are immersed in water, the coupling behavior changes, which induce a re-distribution of the cladding modes. Thus, for the LPFGs fabricated with 192 μm and immersed in water, the $LP_{1,12}$ mode exhibits two resonances around the TAP region at $\sim$1374.4 and $\sim$1523.7 nm

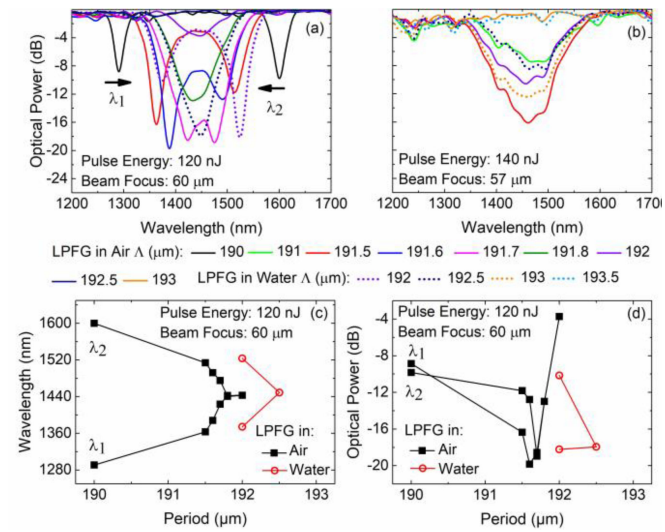

Fig. 3. Transmission spectra of the LPFGs fabricated at a depth of (a) 60 μm with pulse energies of 120 nJ and (b) 57 μm with pulse energies of 140 nJ; (c) resonance wavelengths; (d) optical power versus the grating period for fabrication at a depth of 60 μm with a pulse energy of 120 nJ.

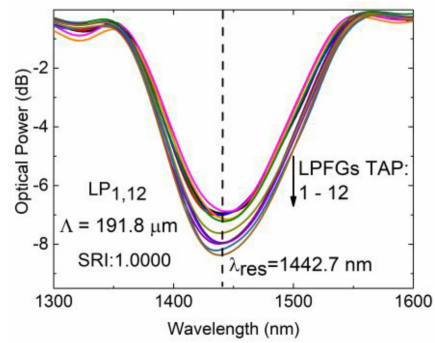

Fig. 4. Fs-laser TAP LPFGs inscribed with a period of 191.8 μm and numbered from 1 to 12.

TABLE I
MAIN CHARACTERISTICS OF THE SET OF LPFGS FABRICATED BY FS-LASER

Values	λ_{res} (nm)	Intensity (dB)	FWHM (nm)
Average	1442.7	-7.6	115.2
Standard Deviation	1.0	0.4	3.5

($\Delta\lambda = 149.3$ nm). The LPFGs operation at the TAP in water was achieved with a grating inscription period of 192.5 μm. In summary, for the grating periods of 191.8 and 192.5 μm, it was verified that the $LP_{1,12}$ mode exhibits a TAP at $\sim$1442.7 and $\sim$1448.6 nm in air and water, respectively.

In order to improve the amplitude of the LPFGs attenuation band, the fs-laser pulse energy was increased to 140 nJ, and the laser beam focus adjusted at a depth of 57 μm from the top center position of the fiber cladding. This procedure allowed the RI modification across the entire core center, as shown in the inset of Fig. 2(b). The difference between the effective RIs of the core and cladding modes increased, and the underlying RI modification induced a change in the coupling behavior leading to a re-distribution of the cladding modes. For this writing condition, the LPFGs operation at the TAP was achieved with grating inscription periods of 192 μm in air and 193 μm in water, resulting in resonance wavelengths at $\sim$1451.1 and $\sim$1453.8 nm, respectively. In addition, the coupling efficiency was improved for the 192 μm LPFG in air, resulting in an -3.1 dB increase of the attenuation band, in comparison with the attenuation band value ($I_{res} = -13.0$ dB) of the 191.8 μm LPFG. However, as can be seen in Fig. 3(b), additional peaks appear on the LPFGs resonance for this writing condition. These additional peaks can be due to the coupling to the higher-order cladding modes, which rely on the sharp inhomogeneities as well as the position and asymmetrical shape of the induced RI modification. In [33], it was theoretically and experimentally determined that the additional peaks were mainly caused by decentered and homogeneously RI modification induced in the fiber core. The grating inscription with an offset of 0.8 μm on the X-axis makes coupling occurs to the asymmetric higher-order cladding modes, where the additional peaks appear between the main resonances. The suppression of these additional peaks can be achieved inducing homogeneous and centered RI modifications in the fiber core, which results in the coupling to the symmetric cladding modes, as reported in [33], [34].

As can be seen in Fig. 3(a), the fabrication of TAP LPFGs without additional peaks in the transmission spectra and coupling to asymmetric modes was achieved due to the position, asymmetry, and elliptic shape of the induced RI modification, depicted in the inset of Fig. 2(a). LPFGs fabricated with longer periods, which allow coupling to the asymmetric $LP_{1,6}$ cladding mode, without additional peaks in the transmission spectrum, were also reported in our previous works [11], [35].

In order to assess the reproducibility of the fs-laser direct writing, twelve LPFGs operating at the TAP region were fabricated with the same fabrication conditions. Figure 4 shows the transmission spectra of twelve TAP LPFGs fabricated with a period of 191.8 μm.

The wavelength, the intensity, and the full width at half maximum (FWHM) of the resonance bands are summarized in Table I. Accordingly, it may be claimed the reproducibility of the fabrication process. The intensity reproducibility was the most challenging parameter to achieve. However, the variation in intensity between devices is not critical for RI sensing. Precise fabrication of fs-laser LPFGs operating at the TAP relies on the sub-micron period control, pulse energy, focal position of the laser beam as well as the fiber tension during fabrication.

The LPFGs sensitivity to the SRI could be further improved by selecting the optimum TiO_2 film thickness for a specific cladding mode. Thus, the behavior of the effective index of the asymmetric $LP_{1,12}$ cladding mode as a function of the TiO_2 film thicknesses was characterized through a 2D analysis of the optical fiber structure and the electromagnetic field modes using the mode analysis of the COMSOL Multiphysics.

The optical fiber structure (SMF-28e, Corning) with four concentric layers was simulated, and the parameters value are presented in Table II. The Sellmeier coefficients for germanium-doped silica [36] and silica [37] were used to calculate the core and cladding RIs at 1442.7 nm, respectively, given by the

TABLE II
FIBER PARAMETERS USED IN THE SIMULATION

Parameter	Core	Cladding	TiO_2 film thickness	SRI
Radius (μm)	4.1	62.5	0.04 – 0.24	200.0
RI	1.4515	1.4453	2.4567	1.0000

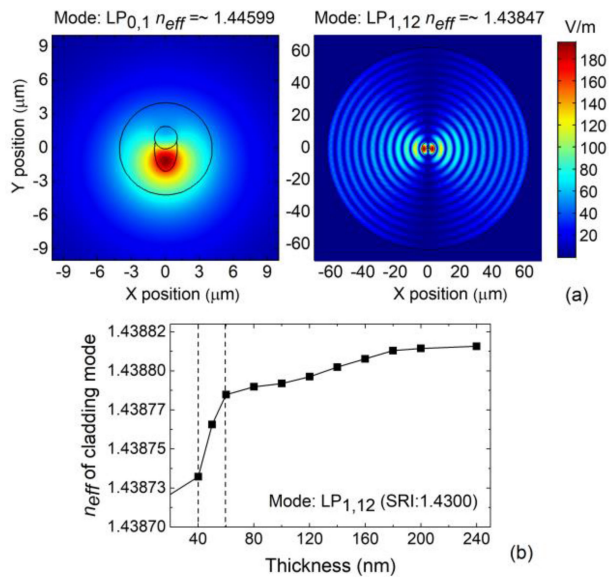

Fig. 5. Simulated, (a) mode profiles (electric field norm) for the $LP_{0,1}$ and $LP_{1,12}$ modes, respectively, considering the LPFG surrounded by air and (b) effective RI of the $LP_{1,12}$ cladding mode as a function of the TiO_2 film thickness for a SRI of 1.4300.

Sellmeier relation reported in [36]. According to DeVore's empirical formula [38], the refractive index of TiO_2 film thickness at 1442.7 nm was determined.

The fs-laser induced RI variation (resembling an elliptic depicted in the inset of Fig. 2(a)), in relation to the core, of the reduced (located above) and increased (located under) RI regions were set to -0.025 and 0.009, respectively.

These values were determined by the measurements of the RI profile at 980 nm with an IFA-100 (Interfiber Analysis) interferometric system. The dimension used in the structure design tried to represent as close as possible the fs-laser induce RI modification cross-section.

The mode profiles of the $LP_{0,1}$ and $LP_{1,12}$ modes, at a wavelength of 1442.7 nm were evaluated, as shown in Fig. 5(a), yielding effective mode indices of $\sim$1.44599 and $\sim$1.43847, respectively. These values yield a grating period of 191.8 μm given by equation 1, which was corroborated by the experimental results, where for the same inscription period, the coupling occurs to the asymmetric $LP_{1,12}$ cladding mode.

Fig. 5(b) shows the variation of the effective RI of the $LP_{1,12}$ mode as a function of the TiO_2 film thickness for a SRI of 1.4300. The simulation was performed for a SRI closer to the cladding material to increase the interaction between the cladding mode and the external medium. The transition region occurs approximately in the range between 40 to 60 nm, as shown in Fig. 5(b). Otherwise, for TiO_2 film thicknesses above approximately 60 nm, the effective RI change stabilizes. However, in a more detailed analysis, the highest effective RI change as a function of the TiO_2 film thickness can be observed for a thickness between 40 to 50 nm. Therefore, for LPFGs fabricated with periods between 198.6 to 199.5 μm, and operating at the TAP in an SRI of 1.4300, the optimum TiO_2 film thickness is between 40 to 50 nm. The evolution of the effective RI as a function of TiO_2 film thickness observed is similar to the one reported in [24], [39], [40]. The behavior of the symmetric $LP_{0,10}$ cladding mode, as a function of the TiO_2 film thickness was verified by simulation and experimentally in [16], and the transition region is located between 60 to 80 nm. Thus, the transition regions rely on the grating fabrication period, the order of the coupling mode, and the SRI of interest underlying the film thickness [16], [24], [25]. The simulation (COMSOL Multiphysics software, version 5.3a) for TiO_2 film thicknesses lower than 40 nm was hampered by compilation issues concerning the minimum mesh size. Consequently, the experimental results demonstrated here could not be replicated theoretically. The mesh was defined by creating free triangular nodes with an extremely fine element size. However, this mesh does not adapt well to the curved geometry of the TiO_2 film for thicknesses lower than 40 nm, leading to inaccurate results (apparently, recent versions of the software used tackle this issue). Experimentally, the fabricated devices could use thicker TiO_2 films at a cost of a lower sensitivity since the resonances would move away from the TAP. Therefore, the devices can be optimized by increasing the film thickness and adjusting the grating period accordingly in order to maintain the grating very close to the TAP, thus ensuring high sensitivity.

The high RI of TiO_2 film coating promotes a quicker transition between cladding guided modes in overlay guided modes [41]. Therefore, LPFGs fabricated with periods to operate at TAP in air and in water were coated with TiO_2 thin films with a thickness of 10, 20, and 30 nm. The thickness of the coated LPFGs was selected to allow the operation very close to the TAP. This causes a coupling behavior change, which leads to a wavelength and intensity shift of the TAP LPFGs resonances. Table III presents the wavelength and intensity shifts for each LPFGs after coating. The resonance band split into two after coating, and the separation between the two resonances increases with the TiO_2 film thickness. Furthermore, a decrease of the attenuation band was observed when the TiO_2 thicknesses increased, more pronounced for the attenuation band ($I_{\lambda 1}$) of the 192.5 μm LPFG. The wavelength and intensity shifts also depend on the slope of the characteristic curve of the resonance band.

B. Refractive Index Sensing

The wavelength sensitivity to the SRI, between 1.0000 and 1.4480, was assessed for the LPFGs fabricated with periods of 191.8 and 192.5 μm, uncoated (bare), and also coated with TiO_2 film thickness of 10, 20, and 30 nm. For clearness, few of the acquired spectra are shown in Fig. 6(a) and (b) for the uncoated 191.8 and 192.5 μm LPFGs, and in Fig. 6(c) and (d) for the 191.8 and 192.5 μm LPFGs coated with 10 and 20 nm thick TiO_2 films, respectively.

As can be seen in Fig. 6, the separation between the two resonances increases with the increase of the TiO_2 thickness, and with the SRI. The LPFGs fabricated with a period of 192.5 μm allows the measurement of a broader RI range, which is restricted

TABLE III
SUMMARY OF THE SPECTRAL CHARACTERISTICS OF THE TiO_2 TAP LPFGS

SRI	Λ (μm)	λ_{res} (nm)	I_{res} (dB)	TiO_2 (nm)	$\Delta\lambda_{res}$ (nm)		ΔI_{res} (dB)	
					λ_1	λ_2	$I_{\lambda 1}$	$I_{\lambda 2}$
1.0000	191.8	1442.7	-10.6	10.0	-64.3	52.0	-1.3	1.9
				20.0	-77.0	63.9	-0.5	3.2
1.3330	192.5	1448.6	-15.6	10.0	-36.3	42.4	1.8	-1.9
				20.0	-55.6	58.3	2.8	-2.1
				30.0	-88.8	95.2	4.7	-0.4

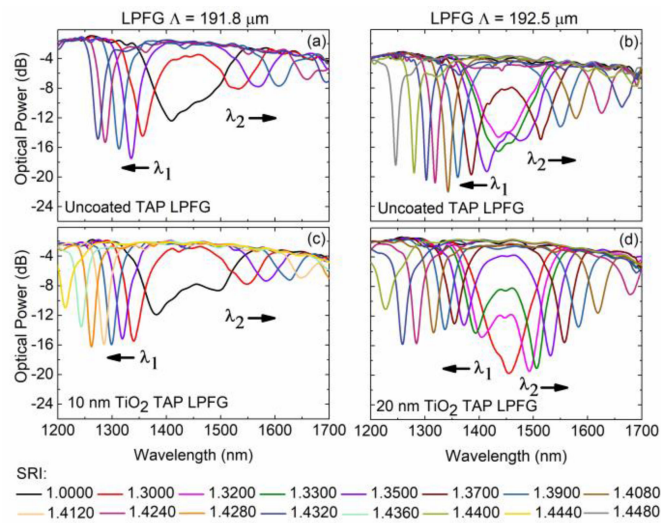

Fig. 6. Transmission spectra of LPFGs fabricated with a period of 191.8 and 192.5 μm, (a) and (b) uncoated, and (c) and (d) coated with 10 and 20 nm thick TiO_2 film, respectively for several values of the surrounding refractive index.

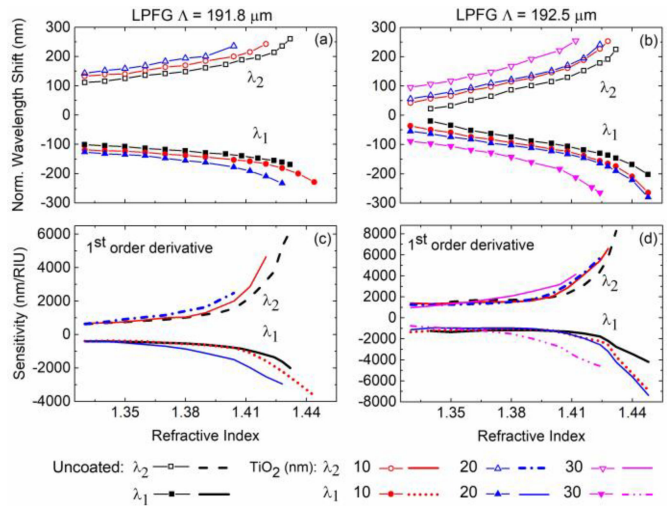

Fig. 7. Normalized wavelength shift (a) and (b), and wavelength sensitivity (c) and (d) of the uncoated and coated with different TiO_2 films thickness for LPFGs fabricated with a period of 191.8 and 192.5 μm as a function of the surrounding refractive index.

by the wavelength measurement range, in this case, up to SRI value of 1.4320 for the both uncoated LPFGs. For the coated LPFGs, the dual-wavelength resonance measurement was restricted to SRI values lower than 1.4320. The increase of the coating thickness induces broader wavelength shift for a given SRI, which is more noticeable for the wavelength resonance, λ_2.

The normalized wavelengths shifts as a function of the SRI, from 1.3300 to 1.4480, are shown in Fig. 7(a) and (b) for the 191.8 and 192.5 μm LPFGs uncoated and TiO_2 coated, respectively. The wavelength response is not linear for this RI range. Thus, the first derivative of the data plotted in Fig. 7(a) and (b) were calculated to assess the wavelength sensitivity.

In the RI range between 1.3700 to 1.4080, the 191.8 μm coated LPFGs presents a wavelength sensitivity increase to SRI, larger for thicker coating thicknesses. The dual-wavelength resonance measurement was defined as the total wavelength shift between the two resonances ($\Delta\lambda = \lambda_2 - \lambda_1$).

The LPFG coated with 20 nm TiO_2 thickness, presents a maximum wavelength sensitivity of -1583.5, and 2560.7 nm/RIU for the resonances λ_1 and λ_2, respectively. Therefore, a sensitivity value of 4144.2 nm/RIU was reached at a RI of 1.4040.

The 191.8 μm LPFG coated with 10 nm thick TiO_2 film, reached a wavelength sensitivity of 6351.1 nm/RIU ($\lambda_1 = -1611.6$, and $\lambda_2 = 4739.5$ nm/RIU) at a RI of 1.4200. However, the maximum wavelength sensitivity of 8169.8 nm/RIU ($\lambda_1 = -2020.6$, and $\lambda_2 = 6149.2$ nm/RIU) at a RI of 1.4320 was found for the uncoated 191.8 μm LPFG. For the 192.5 μm LPFGs a maximum wavelength sensitivity value of 11257.5 nm/RIU ($\lambda_1 = 2876.8$, and $\lambda_2 = 8380.7$ nm/RIU) at a RI of 1.4320 was found for the uncoated LPFG. Therefore, it can be seen that the uncoated 192.5 μm LPFG sensitivity was improved by a factor of $\sim$1.4 in comparison to the 191.8 μm LPFG. However, for the 192.5 μm LPFG, it was seen a wavelength sensitivity decrease with the increase of the TiO_2 coating thickness for RI higher than 1.4120. This was due to the impossibility of dual-wavelength resonance measurement (resonance λ_2 outside of the measurement range). As such, the LPFG coated with 10 nm TiO_2 thickness, reached a wavelength sensitivity of 9117.1 nm/RIU ($\lambda_1 = -2580.8$, and $\lambda_2 = 6536.3$ nm/RIU) at a RI of 1.4280. Regarding the LPFG coated with 20 nm TiO_2 thickness, a wavelength sensitivity of 8347.4 nm/RIU ($\lambda_1 = -2553.4$, and $\lambda_2 = 5794.0$ nm/RIU) at a RI of 1.4240 was achieved. In the RI between 1.3700 to 1.4120 (upper limit for dual-wavelength measurement) for all LPFGs, the maximum wavelength sensitivity of 8051.4 nm/RIU ($\lambda 1 = -3773.9$, and $\lambda 2 = 4277.5$ nm/RIU) was achieved for the LPFG coated with 30 nm of TiO_2. It can be seen that the sensitivity enhancement depends on the fabrication period, which allows operating closer to the TAP region at a specific RI, where the sensitivity reaches maximum values. Furthermore, for SRI closer to the cladding RI of the SMF-28e fiber, i.e., $n_D{}^{25°C} = 1.4540$, cladding modes interact more with the external medium, leading to the increase

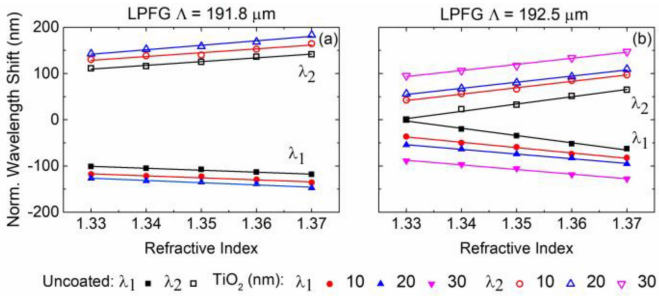

Fig. 8. Normalized wavelength shift (a) and (b) for the uncoated LPFGs and coated with different thick TiO_2 films fabricated with a period of 191.8 and 192.5 μm, respectively in the RI range of water-based solutions. Experimental data points were fitted to a linear equation.

TABLE IV
WAVELENGTH SENSITIVITY FOR BARE AND TiO_2 COATED LPFGS IN THE RI RANGE OF WATER-BASED SOLUTIONS

Λ (μm)	TiO_2 (nm)	SENSITIVITY (nm/RIU)		LINEARITY (R^2)	
		λ_1	λ_2	λ_1	λ_2
191.8	Bare	-421.4 ± 27.9	813.0 ± 57.4	0.99	
		Δλ = 1234.4 ± 72.2			
	10.0	-437.6 ± 58.6	827.3 ± 84.8	0.95	
		Δλ = 1264.9 ± 173.4		0.93	
	20.0	-487.0 ± 53.7	971.0 ± 85.6	0.96	0.98
		Δλ = 1458.0 ± 137.2		0.97	
192.5	Bare	-1571.9 ± 90.6	1579.9 ± 99.6	0.99	
		Δλ = 3151.8 ± 177.0			
	10.0	-1156.3 ± 56.3	1382.9 ± 70.4		
		Δλ = 2539.2 ± 177.7			
	20.0	-1012.0 ± 39.5	1325.0 ± 54.8		
		Δλ = 2337.0 ± 91.2			
	30.0	-1001.5 ± 50.8	1319.3 ± 65.7		
		Δλ = 2320.8 ± 115.4			

of the LPFG sensitivity. However, the increase of the LPFG sensitivity for the RI range between 1.3700 − 1.4120, was mainly caused by the increase of the TiO_2 film thickness, which enhanced the evanescent wave interaction with the surrounding medium.

The normalized wavelengths shift to SRI in the range between 1.3300 to 1.3700 (i.e., around water-based solutions) was also determined, as depicted in Fig. 8. Although the wavelength response to the SRI presents a nonlinear trend, in a narrow SRI range it can be considered linear. Thus a linear fit was applied to the results in Fig. 8 in order to assess the wavelength sensitivity (average ± standard deviation), presented in Table IV.

For the 191.8 μm LPFGs, the wavelength sensitivity in the RI range of water-based solutions was improved, being higher for larger TiO_2 film thickness. As such, a maximum average wavelength sensitivity of 1458.0 ± 137.2 nm/RIU ($\lambda_1 = -487.0 \pm 53.7$, and $\lambda_2 = 971.0 \pm 85.6$ nm/RIU) was achieved for the LPFG coated with 20 nm TiO_2 thickness.

For the 191.8 μm LPFGs operation occurs far away from TAP for SRI around water solutions. In this zone of the phase-matching curve, it was found that the TiO_2 coating improves the wavelength sensitivity. Thus, the proper choice of the LPFGs period allows the tuning of the operation at the TAP, which

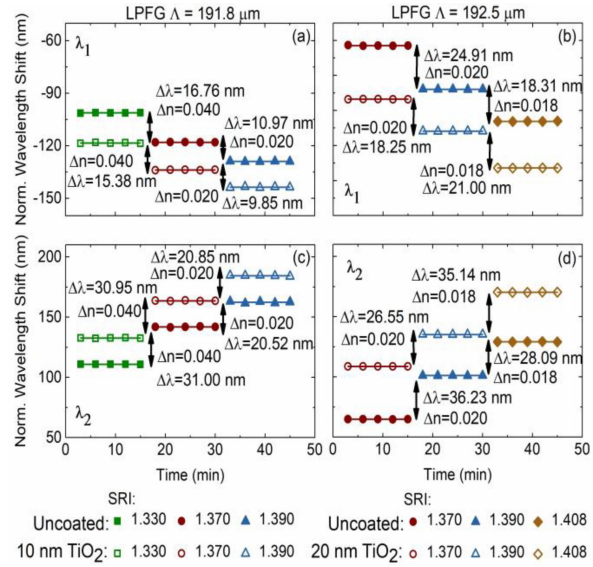

Fig. 9. Normalized wavelength shift as a function of time when the surrounding medium undertakes step variations for the resonance: (a) and (b) λ_1, and (c) and (d) λ_2 of the LPFGs fabricated with a period of 191.8 and 192.5 μm, respectively.

TABLE V
RI RESOLUTIONS FOR THE BARE AND TiO_2 COATED LPFGS

Λ (μm)	TiO_2 (nm)	STEP	RI RESOLUTIONS	
			λ_1	λ_2
191.8	Bare	1	1.7×10^{-4}	2.7×10^{-4}
		2	2.3×10^{-4}	5.9×10^{-4}
	10.0	1	5.7×10^{-4}	2.7×10^{-4}
		2	4.3×10^{-4}	3.1×10^{-4}
192.5	Bare	1	1.3×10^{-5}	4.3×10^{-5}
		2	8.2×10^{-5}	6.8×10^{-5}
	20.0	1	8.8×10^{-5}	8.2×10^{-5}
		2	6.9×10^{-5}	5.6×10^{-5}

improves the wavelength sensitivity of the bare and coated LPFGs.

However, for the 192.5 μm LPFGs, it was found that the wavelength sensitivity decreases with the increase of the TiO_2 coating. Indeed, a maximum average wavelength sensitivity of 3151.8 ± 177.0 nm/RIU ($\lambda_1 = -1571.9 \pm 90.6$, and $\lambda_2 = 1579.9 \pm 99.6$ nm/RIU) was achieved for the bare 192.5 μm LPFG. In addition, considering a narrow RI between 1.3300 to 1.3400, the bare 192.5 μm LPFG reaches a wavelength sensitivity of 4294.5 nm/RIU ($\lambda_1 = -2038.0$, and $\lambda_2 = 2256.5$ nm/RIU).

The wavelengths sensitivity achieved for each LPFG relies on the TiO_2 coating thickness, which by changing the effective indices of the cladding modes induces a shift in the wavelength position of each TAP LPFG. Therefore, it causes the single resonance band to split into two distinct resonances and, consequently, the sensitivity of the TAP LPFGs decreases.

The choice of a 192.5 μm fabrication period for an uncoated LPFG allowed the operation at the TAP for RI around water-based solutions, enhancing the wavelength sensitivity to the SRI. The fine-tuning of the LPFG fabrication period to values higher than 192.5 μm, in conjunction with an adequate choice of the

TABLE VI
COMPARISON BETWEEN THE SENSITIVITY DISPLAYED BY LPFGS OPERATING AROUND TAP REPORTED IN THE LITERATURE AND THIS WORK

FABRICATION PROCESS	SENSITIVITY (NM/RIU)	RI RANGE	REFERENCES
1. EXCIMER LASER POINT BY POINT EXPOSURE; 2. CHEMICAL ETCHING.	6269.2	1.3300 - 1.3400	[42,43]
1. EXCIMER LASER AND AMPLITUDE CHROMIUM MASK; 2. CHEMICAL ETCHING; 3. COATING WITH TiO_2.	6200.0	1.3400	[24]
	4300.0	1.3600-1.4100	
1. EXCIMER LASER AND AMPLITUDE CHROMIUM MASK; 2. CHEMICAL ETCHING; 3. COATING WITH DIAMOND-LIKE CARBON.	22000.0	1.3344 - 1.3355	[48]
	2000.0	1.3400 - 1.3560	
THEORETICAL WORK: 1. CHEMICAL ETCHING; 2. COATING WITH THIN-FILM.	3750.0	1.3300 - 1.3500	[44]
	143000.0	1.3300-1.3310	
1. EXCIMER LASER POINT BY POINT EXPOSURE; 2. CHEMICAL ETCHING; 3. COATING WITH POLY ALLYLAMINE HYDROCHLORIDE/POLY ACRYLIC ACID.	5602.0	1.3700 - 1.4100	[45,47]
1. EXCIMER LASER POINT BY POINT EXPOSURE; 2. SOL-GEL BASED TITANIA-SILICA THIN FILM OVERLAY.	7075.3	1.3330 – 1.3340	[25]
1. CHEMICAL ETCHING; 2. COATING WITH TIN DIOXIDE (SnO_2). 3. PERIODIC LASER ABLATION.	6430.0	1.3740 - 1.3890	[7]
ELECTRIC ARC DISCHARGES	590.0	1.3300 - 1.4200	[6]
FEMTOSECOND LASER DIRECT WRITTEN	930.0	1.3330 - 1.3980	[46]
1. FEMTOSECOND LASER DIRECT WRITTEN; 2. COATING WITH TiO_2.	3151.7	1.3300 - 1.3700	THIS WORK
	4294.5	1.3300 - 1.3400	
	11257.4	1.4320	
	8051.4	1.3700 - 1.4120	

This comparison was restricted to the LPFGs operating around the TAP and fabricated in the SMF-28 fiber.

TiO_2 film thickness, will allow the operation at TAP for SRI around water-based solutions.

The analysis of the spectral resolution was done as described in the section material and methods, and the data concerning the SRI step variations are shown in Fig. 9. Table V presents the calculated RI resolutions for the bare and TiO_2 coated LPFGs. Refractive index resolutions with magnitudes of 10^{-4} and 10^{-5} RIU were achieved for the LPFGs fabricated with a period of 191.8 and 192.5 μm, respectively.

Finally, a comparison between the LPFGs fabricated in SMF-28 fibers operating at the TAP reported in the literature and the ones developed in this work was realized and summarized in Table VI.

Thus, among the few LPFGs fabricated in SMF-28 fibers reported operating at the TAP, the LPFGs fabricated on this work exhibited higher sensitivity in comparison to the LPFGs fabricated by electric-arc, fs-laser direct written and also excimer laser exposure.

Nevertheless, the maximum sensitivity (i.e., 143000 nm/RIU for a very narrow RI range between 1.3300 to 1.3310, [44]) was theoretically achieved for the TAP LPFGs with reduced cladding diameter and coated with a thin film. Experimentally, a sensitivity over 22000 nm/RIU for a very narrow RI range between 1.3344 to 1.3355 was reported for the TAP LPFGs with reduced cladding diameter and coated with a diamond-like carbon thin film [48]. The demonstrated LPFGs sensitivity enhancement relies mainly on the evanescent interaction achieved by reducing the cladding diameter. However, this approach involves a complex fabrication process to tune the LPFG operation at the TAP and makes the optical fiber fragile and difficult to handling. The fabrication process proposed in this work allows optimizing the LPFGs sensitivity to the SRI without making the optical fiber fragile in comparison to the fabrication process using chemical etching.

Indeed, the increase of the LPFGs sensitivity for SRI closer to 1.4300, mainly caused by the increase of the TiO_2 film thickness, makes them suitable, for example, for the detection of fuel adulteration (kerosene in petrol), which leads to air pollution and the consequent effects on public health. The refractive index of pure petrol and kerosene are 1.4270 and 1.4420, respectively [31]. The LPFGs can also be coated with a polymer engineered to be sensitive to external parameters, and having a RI close to the value where the highest sensitivity was obtained, and that changes with the ambient humidity or the presence of a specific gas, for example [25]. LPFGs operating at the TAP inscribed by a CO_2 laser in B-Ge doped fiber for fuel adulteration detection was reported in [49]. Here, an average grating sensitivity of 1635.0 nm/RIU for SRI in the range between 1.3970 to 1.4372 has been demonstrated. Nevertheless, a maximum wavelength sensitivity value of 11257.5 nm/RIU at a RI of 1.4320 was

reported in our work. Therefore, it can be seen that the LPFG sensitivity was improved by a factor of ∼6.9 in comparison to TAP inscribed by a CO2 laser [49].

IV. Conclusion

The precise production of LPFGs operating at the TAP in an SMF-28e fiber through fs-laser direct writing was demonstrated. The inscription of LPFGs with a clear spectrum without higher-order interference peaks was achieved by writing RI modification with a laser pulse energy of 120 nJ at a depth of 60 μm from the top center position of the fiber cladding. The LPFGs operating at the TAP of the asymmetric $LP_{1,12}$ cladding mode in air and water were fabricated with an RI modulation period of 191.8 and 192.5 μm, yielding a resonance wavelength at approximately 1442.7 and 1448.6 nm, respectively. It was demonstrated that the precise fabrication of the fs-laser LPFGs operating at the TAP relies on the sub-micron period control, the pulse energy, the focal position of the laser beam as well as the fiber tension during fabrication. The LPFGs were coated with different TiO_2 film thickness to improve the sensitivity to SRI, and their spectral behavior around the TAP in air and water characterized. The wavelength sensitivity to the SRI was also assessed. Therefore, a maximum sensitivity of ∼8051.4 nm/RIU in the range between 1.3700 to 1.4120 was obtained for the 192.5 μm LPFG coated with 30 nm TiO_2 thickness. The maximum sensitivity in the RI range of water-based solutions was approximately 3151.7 nm/RIU, achieved for the uncoated 192.5 μm LPFG. The SRI sensitivity could be further improved, tuning the LPFG fabrication period to operate at the TAP accordingly to the TiO_2 film thickness.

Another approach could be to tune the operation at TAP by reducing the cladding diameter and posteriorly coating with different TiO_2 film thickness. Further works are ongoing in order to optimize the fs-laser TAP LPFGs, which will be essential to the suitable application in the biological, chemical, or biochemical sensing applications.

References

[1] N. Jovanovic, A. Fuerbach, G. D. Marshall, M. Ams, and M. J. Withford, "Femtosecond Laser Micromachining: Photonic Microfluidic Devices Transparent Materials," in *Topics in Applied Physics*, Berlin, Heidelberg: Springer, 2012, doi: 10.1007/978-3-642-23366-1_8.

[2] X. Lan *et al.*, "Turn-around point long-period fiber grating fabricated by CO_2 laser for refractive index sensing," *Sensors Actuators, B Chem.,* vol. 177, pp. 1149–1155, 2013.

[3] X. Lan, Q. Han, T. Wei, J. Huang, and H. Xiao, "Turn-around-point long-period fiber gratings fabricated by CO laser point-by-point irradiations," *IEEE Photon. Technol. Lett.*, vol. 23, no. 22, pp. 1664–1666, Nov. 2011.

[4] R. Y. N. Wong, E. Chehura, S. E. Staines, S. W. James, and R. P. Tatam, "Fabrication of fiber optic long period gratings operating at the phase matching turning point using an ultraviolet laser," *Appl. Opt.*, vol. 53, no. 21, 2014, Art. no. 4669.

[5] R. M. Carter *et al.*, "Experimental difficulties with LPG sensors operating close to the phase turning points," *J. Lightw. Technol.*, vol. 34, no. 17, pp. 3999–4004, Sep. 2016.

[6] C. Colaço, P. Caldas, I. Del Villar, R. Chibante, and G. Rego, "Arc-induced long-period fiber gratings in the dispersion turning points," *J. Lightw. Technol.*, vol. 34, no. 19, pp. 4584–4590, Oct. 2016.

[7] J. Ascorbe, J. M. Corres, I. del Villar, and I. R. Matias, "Fabrication of long period gratings by periodically removing the coating of cladding-etched single mode optical fiber towards optical fiber sensor development," *Sensors*, vol. 18, no. 6, p. 1866, Jun. 2018.

[8] S. W. James and R. P. Tatam, "Optical fibre long-period grating sensors: Characteristics and application," *Meas. Sci. Technol.*, vol. 14, no. 5, pp. R49–R61, 2003.

[9] Y. Kondo, K. Nouchi, T. Mitsuyu, M. Watanabe, P. G. Kazansky, and K. Hirao, "Fabrication of long-period fiber gratings by focused irradiation of infrared femtosecond laser pulses," *Opt. Lett.*, vol. 24, no. 10, pp. 646–648, 1999.

[10] Y. Zhang *et al.*, "Sensing characteristics of long period grating by writing directly in SMF-28 based on 800 nm femtosecond laser pulses," *Opt. Laser Technol.*, vol. 121, Jun., 2020, Art. no. 105839.

[11] D. Viveiros *et al.*, "Temperature stability and spectral tuning of long period fiber gratings fabricated by femtosecond laser direct writing," *Sensors*, vol. 20, no. 14, Jul. 2020, Art. no. 3898.

[12] S. Liu, M. Luo, and Q. Ji, "Sensing characteristics of femtosecond laser-induced long period gratings by filling cladding holes in photonic crystal fiber," *J. Lightw. Technol.*, vol. 32, no. 12, pp. 2287–2292, Jun. 2014.

[13] A. A. Wolf, A. V. Dostovalov, I. A. Lobach, and S. A. Babin, "Femtosecond laser inscription of long-period fiber gratings in a polarization-maintaining fiber," *J. Lightw. Technol.*, vol. 33, no. 24, pp. 5178–5183, Dec. 2015.

[14] A. I. Kalachev, D. N. Nikogosyan, and G. Brambilla, "Long-period fiber grating fabrication by high-intensity femtosecond pulses at 211 nm," *J. Lightw. Technol.*, vol. 23, no. 8, pp. 2568–2578, Aug. 2005.

[15] X. Shu, L. Zhang, and I. Bennion, "Sensitivity characteristics of long-period fiber gratings," *J. Lightw. Technol.*, vol. 20, no. 2, pp. 255–266, Feb. 2002.

[16] F. Zou, Y. Liu, C. Mou, and S. Zhu, "Optimization of refractive index sensitivity in nanofilm-coated long-period fiber gratings near," *J. Lightw. Technol.*, vol. 38, no. 4, pp. 889–897, Feb. 2020.

[17] F. Chiavaioli *et al.*, "Towards sensitive label-free immunosensing by means of turn-around point long period fiber gratings," *Biosens. Bioelectron.*, vol. 60, pp. 305–310, 2014.

[18] Ś. Mateusz, M. Koba, P. Mikulic, and W. J. Bock, "Towards refractive index sensitivity of long- period gratings at level of tens of μm per refractive index unit : Fiber cladding etching and nano-coating deposition," *Opt. Express*, vol. 24, no. 11, pp. 11897–11904, 2016.

[19] T. K. Dey *et al.*, "Analysis of the lowest order cladding mode of long period fiber gratings near turn around point," in *J. Lightw. Technol.*, 2020, doi: 10.1109/JLT.2020.2987795.

[20] A. Cusano *et al.*, "Mode transition in high refractive index coated long period gratings," *Opt. Exp.*, vol. 14, no. 1, pp. 19–34, 2006.

[21] P. Pilla, C. Trono, F. Baldini, F. Chiavaioli, M. Giordano, and A. Cusano, "Giant sensitivity of long period gratings in transition mode near the dispersion turning point : An integrated design approach," *Opt. Lett.*, vol. 37, no. 19, pp. 4152–4154, 2012.

[22] X. Liu, M. Yan, L. Zhan, S. Luo, Z. Zhang, and Y. Xia, "Controlling of symmetric and asymmetric mode coupling in long-period fiber gratings singe-side induced by long-pulse CO2 laser," *Opt. Commun.*, vol. 284, no. 5, pp. 1232–1237, 2011.

[23] M. Heck *et al.*, "Control of higher-order cladding mode excitation with tailored femtosecond-written long period fiber gratings," *Opt. Exp.*, vol. 27, no. 4, 2019, Art. no. 4292.

[24] M. Smietana *et al.*, "Label-free sensitivity of long-period gratings enhanced by atomic layer deposited tio2 nano-overlays," *Opt. Exp.*, vol. 23, no. 7, 2015, Art. no. 8441.

[25] F. Chiavaioli *et al.*, "Sol-gel-based titania-silica thin film overlay for long period fiber grating-based biosensors," *Anal. Chem.*, vol. 87, no. 24, pp. 12024–12031, 2015.

[26] K. Krogulski *et al.*, "Effect of tio2 nano-overlays deposited with atomic layer deposition on refractive index sensitivity of long-period gratings," *Proc. Int. Conf. Sens. Technol.*, no. 1, pp. 573–577, 2014.

[27] L. Coelho, J. L. Santos, D. Viegas, and J. M. M. M. de Almeida, "Fabrication and characterization of metal oxide-coated long-period fiber gratings," *J. Lightw. Technol.*, vol. 34, no. 10, pp. 2533–2539, May 2016.

[28] L. Coelho, D. Viegas, J. L. Santos, J. De Almeida, and J. M. M. M. De Almeida, "Enhanced refractive index sensing characteristics of optical fibre long period grating coated with titanium dioxide thin films," *Sensors Actuators B Chem.,* vol. 202, pp. 929–934, 2014.

[29] L. Coelho, D. Viegas, J. L. Santos, and J. M. M. M. De Almeida, "Optical sensor based on hybrid FBG/titanium dioxide coated LPFG for monitoring organic solvents in edible oils," *Talanta*, vol. 148, pp. 170–176, 2016.

[30] H. C. A. S. G. Vasconcelos, J. M. M. M. de Almeida, C. M. T. Saraiva, P. A. da S. Jorge, and L. C. C. Coelho, "Mach–Zehnder interferometers based on long period fiber grating coated with titanium dioxide for refractive index sensing," *J. Lightw. Technol.*, vol. 37, no. 18, pp. 4584–4589, Sep. 2019.

[31] Y. Singh, T. Iqbal, and S. K. Raghuwanshi, "Fuel adulteration detection system using etched clad based fiber bragg grating (FBG) sensor," in *Proc. Opt. Sens. Detection VI*, Apr. 1, 2020, pp. 113542T-1–113542T-6, doi: 10.1117/12.2556814.

[32] F. Chiavaioli, C. A. J. Gouveia, P. A. S. Jorge, and F. Baldini, "Towards a uniform metrological assessment of grating-based optical fiber sensors: From refractometers to biosensors," *Biosensors*, vol. 7, no. 2:23, pp. 7020023-1–7020023-29, 2017, doi: 10.3390/bios7020023.

[33] M. Heck *et al.*, "Control of higher-order cladding mode excitation with tailored femtosecond-written long period fiber gratings," *Opt. Exp.*, vol. 27, no. 4, pp. 4292–4303, 2019.

[34] A. V. Dostovalov, A. A. Wolf, and S. A. Babin, "Long-period fibre grating writing with a slit-apertured femtosecond laser beam ($\lambda = 1026$ nm)," *Quantum Electron.,* vol. 45, no. 3, pp. 235–239, 2015.

[35] D. Viveiros *et al.*, "Femtosecond laser-written long period fibre gratings coated with titanium dioxide for improved sensitivity," in *Proc. Opt. Sens. Detection VI*, 2020, Art. no. 113540C.

[36] R. Lingle *et al.*, "Light-guiding fundamentals and fiber design," in *Specialty Optical Fibers Handbook*, Nor Cross, Georgia: OFS Corporate R&D, pp. 19–68, 2007, doi: 10.1016/B978-012369406-5/50004-7.

[37] I. H. Malitson, "Interspecimen comparison of the refractive index of fused silica∗,†," *J. Opt. Soc. Amer.*, vol. 55, no. 10, 1965, Art. no. 1205.

[38] A. K. Sharma and G. J. Mohr, "Theoretical understanding of an alternating dielectric multilayer-based fiber optic SPR sensor and its application to gas sensing," *New J. Phys.*, vol. 10, 2008, Art. no. 023039.

[39] M. Smietana, W. J. Bock, and J. Szmidt, "Evolution of optical properties with deposition time of silicon nitride and diamond-like carbon films deposited by radio-frequency plasma-enhanced chemical vapor deposition method," *Thin Solid Films*, vol. 519, no. 19, pp. 6339–6343, 2011.

[40] E. Davies, R. Viitala, M. Salomäki, S. Areva, L. Zhang, and I. Bennion, "Sol-gel derived coating applied to long-period gratings for enhanced refractive index sensing properties," *J. Opt. Pure Appl. Opt.*, vol. 11, no. 1, 2009, Art. no. 015501.

[41] I. Del Villar *et al.*, "Optimization of sensitivity in long period fiber gratings with overlay deposition," *Opt. Exp.*, vol. 13, no. 1, pp. 56–69, 2005.

[42] P. Biswas, N. Basumallick, S. S. Bandyopadhyay, K. Dasgupta, A. Ghosh, and S. S. Bandyopadhyay, "Sensitivity enhancement of turn-around-point long period gratings by tuning initial coupling condition," *IEEE Sens. J.*, vol. 15, no. 2, pp. 1240–1245, Feb. 2015.

[43] T. Eftimov, M. Janik, M. Koba, M. Śmietana, P. Mikulic, and W. Bock, "Long-Period gratings and microcavity in-line Mach Zehnder interferometers as highly sensitive optical fiber platforms for bacteria sensing," *Sensors*, vol. 20, no. 13, 2020, Art. no. 3772.

[44] I. Del Villar, "Ultrahigh-sensitivity sensors based on thin-film coated long period gratings with reduced diameter, in transition mode and near the dispersion turning point," *Opt. Exp.*, vol. 23, no. 7, pp. 8389–8398, 2015.

[45] Q. Ling, Z. Gu, and K. Gao, "Smart design of a long-period fiber grating refractive index sensor based on dual-peak resonance near the phase-matching turning point," *Appl. Opt.*, vol. 57, no. 10, pp. 2693–2697, 2018.

[46] F. Shen, K. Zhou, L. Zhang, and X. Shu, "Long period fiber grating around the dispersion turning point fabricated with a femtosecond laser," *Opt. InfoBase Conf. Paper*, vol. Part F83-A, pp. 20–22, 2017.

[47] Q. Ling, Z. Gu, X. Jiang, and K. Gao, "Design of long period fiber grating surrounding refractive index sensor based on mode transition near phase-matching turning point," *Opt. Commun.*, vol. 439, pp. 187–192, 2019.

[48] M. Śmietana, M. Koba, P. Mikulic, and W. J. Bock, "Combined plasma-based fiber etching and diamond-like carbon nanooverlay deposition for enhancing sensitivity of long-period gratings," *J. Lightw. Technol.*, vol. 34, no. 19, pp. 4615–4619, Oct. 2016.

[49] S. Kher, S. Chaubey, J. Kishore, and S. M. Oak, "Detection of fuel adulteration with high sensitivity using turnaround point long period fiber gratings in B/Ge doped fibers," *IEEE Sens. J.*, vol. 13, no. 11, pp. 4482–4486, Nov. 2013.

Duarte Viveiros received the Graduate degree in electronics and telecommunications engineering and the M.Sc. in energy networks and telecommunications engineering from the University of Madeira, Madeira, Portugal, in 2011 and 2013, respectively. He is currently working toward the Ph.D. degree in physics from the Faculty of Sciences, University of Porto, Porto, Portugal, with the focus on the optical fiber sensors fabricated by femtosecond laser direct writing in collaboration with the Centre for Applied Photonics, INESC TEC, Porto, Portugal. His current research interests include optical sensors, femtosecond laser direct writing techniques for optical fiber and integrated optics, Bragg gratings, and long period gratings.

José Manuel Marques Martins de Almeida received the Graduate degree in applied physics (optics and electronics), the Ph.D. degree from the University of Porto, Porto, Portugal, in 1987 and 1998, respectively, and the Habilitation degree from University de Trás-os-Montes e Alto Douro, Vila Real, Portugal, in 2006. Since 2000, he has been an Associate Professor with the Department of Physics, University de Trás-os-Montes e Alto Douro. He is currently a Researcher Coordinator with the Centre for Applied Photonics of INESC TEC, Porto, Portugal. His current research interests include optical sensors, integrated optics, spectroscopy, and biophysics.

Luís Coelho received the Ph.D. degree in physics from the University of Porto, Porto, Portugal, with the focus on thin films technology applied to optical fiber sensors. In the last few years, he has authored or coauthored more than 67 papers in international journals and more than 68 papers in national and international conferences with more than 2384 citations and h index of 21. His main research interests include the detection and monitoring of chemical entities and biological targets through the application of a wide variety of optical technologies using the effect of fluorescence and absorption or the evanescent field combined with plasmonics. He is currently working in the development of fiber optic probes to real-time monitor pollutants and contaminants on water systems.

Helena Vasconcelos received the Graduate degree in food science and the M.Sc. degree in food safety from the School of Agrarian and Veterinary Sciences, CECAV, University of Trás-os-Montes e Alto Douro Vila Real, Vila Real, Portugal, in 2011 and 2014, respectively. She is currently working toward the Ph.D. degree with the School of Agrarian and Veterinary Sciences, CECAV, University of Trás-os-Montes e Alto Douro, Vila Real, Portugal, in collaboration with the Centre for Applied Photonics of INESC TEC, Porto, Portugal.

João M. Maia received the B.Sc. degree in technological physics and the M.Sc. degree in physics engineering, in 2014 and 2016, respectively, from the Faculty of Sciences, University of Porto, Porto, Portugal, where he is currently working toward the Ph.D. degree in physics. In 2015, he joined the Centre for Applied Photonics, INESC TEC, Porto, Portugal, where he is researching on femtosecond laser micromachining. His current research interests include fabrication of optofluidic devices in fused silica and photopolymerization.

Vítor A. Amorim received the B.Sc. degree in technological physics and the M.Sc. degree in physical engineering from the University of Porto, Porto, Portugal, where, he has been working toward the Ph.D. degree in physics since 2016. In 2015, he joined the Centre for Applied Photonics of INESC TEC, Porto, Portugal, where he is currently enrolled in research activity. His current research interests include integrated optical devices fabricated by femtosecond laser direct writing for sensing applications.

Pedro A. S. Jorge is currently an Assistant Professor with the Department of Physics and Astronomy, University of Porto, Porto, Portugal. Since 2007, he has been a Senior Researcher with the Centre for Applied Photonics, INESC TEC, leading the Biochemical Sensor Group. He has coauthored 90 peer-reviewed papers, three book chapters and more than 200 communications in international and national conferences in the field of optical sensors. He is the author of one patent, and three patent pending (EP).

Paulo V. S. Marques is currently an Associate Professor with the Faculty of Sciences, Physics, and Astronomy Department, Porto University, Porto, Portugal, and since 2009, has been the Coordinator of the Center of Applied Photonics, INESC TEC, Porto, Portugal, and also the Director of Micro and Nanofabrication Center, Porto University. He has authored or coauthored four world patents (patent family of 32), more than 100 scientific papers in international magazines and conferences and three book chapters. His current research interests include optical sensors, femtosecond laser direct writing techniques for integrated optics and microfabrication in general, microfluidics, bragg gratings, and active devices.